J. Fluid Mech. (1986), *vol.* 162, *pp.* 283–298
Printed in Great Britain

Experimental analysis of the pressure field induced on a square cylinder by a turbulent flow

By J. P. HUOT, C. REY† AND H. ARBEY‡

Laboratoire de Mécanique des Fluides, associé au C.N.R.S.,
Ecole Centrale de Lyon, 69130 ECULLY, France

(Received 1 August 1983 and in revised form 23 July 1985)

This paper is devoted to the study of the mean and fluctuating pressure field that develop on the surface of a square cylinder (side D) placed in homogeneous flows with different intensities ($u'/\bar{U}_\infty$) and ratios of turbulence scales to cylinder scale L_{11}/D. In these experiments $u'/\bar{U}_\infty$ varies from 3 to 17.5% and L_{11}/D varies from 0.1 to 2. This range of experimental conditions is more extensive than that of Lee (1975). Lee's results are largely confirmed, in particular the influence of varying turbulence intensity on the mean pressure distribution in the recirculation region is much stronger than that of varying the integral scale. The theory proposed by Durbin & Hunt (1980) for the prediction of the pressure spectrum at the stagnation point has been shown to be adequate for low frequencies but only qualitative at high frequencies. Finally, measurements of cross-spectra, taken for different points on the same cross-section, have shown how the fluctuating surface pressure field downwind of separation has a narrowband component at the Strouhal frequency that is sensitive to the turbulence, and a broadband component generated by the recirculating flow that is insensitive to the upwind turbulence.

1. Introduction

The construction of high-rise towers has focused attention on the effects of wind on such buildings. The response of these structures to the pressure field induced by the atmospheric turbulence is extremely complex. Therefore it has proved necessary to study the various mechanisms using simplified theoretical or experimental models, such as studies performed on primastic cylinders placed in turbulent flows.

In such studies it has proved convenient to decompose the pressure field into mean and fluctuating parts and to study them separately. In addition we shall distinguish two zones: upstream and downstream of the separation of the shear layers. The mean pressure field, upstream of the separation point, is independent of the characteristics of the incident turbulence (Lee 1975; Barriga, Crowe & Robertson 1975), of the blocking ratio and of the geometry of the afterbody in the separated region (Ranga Raju & Vijaya Singh 1975). On the other hand, in the region downstream of the separation point, the pressure coefficient depends on the behaviour of the free-shear layers (Laneville, Gartshore & Parkinson 1975; Courchesne & Laneville 1982; Kwok 1983), on the geometry of the afterbody, on the characteristics of the incident turbulence, on the Reynolds number, and on the blocking coefficient.

The fluctuating pressure field is due to the velocity fluctuations in the incident

† Present address: Ecole Nationale Supérieure de Mécanique – 44072 NANTES.
‡ Present address: Institut National de Recherche et de Sécurité – 54501 VANDOEUVRE.

stream and to various instabilities in the wake region, such as vortex shedding, recirculation, and intermittent reattachments. In the upstream zone the pressure fluctuations, associated with the incoming turbulence, are assumed to be independent of those associated with the wake (Hunt 1973). This pressure field has been studied by Vickery (1966), Bearman (1972), Kao (1970), Lee (1975) and Kawai, Katsura & Ishizaki (1980). However spectral studies of the pressure field on the upstream face are rare. We are only aware of the work of Kao, limited to the low-frequency domain, of Bearman for the stagnation point of a flat plate normal to the flow and that of Kawaī *et al.* Downstream of the separation, the fluctuating pressure field is dominated by vortex shedding and, as a consequence, it has a very energetic periodic component at the Strouhal frequency f_S. The effects of turbulence on this quasi-periodic pressure field have been studied by Vickery (1966) and Lee (1975), for the sides of the prism. In addition, the presence of a reattachment point or intense recirculation in the vicinity of the separation point may cause strong pressure fluctuations in localized zones (Robertson *et al.* 1978; Wedding *et al.* 1978).

To predict the fluctuating pressure field induced by the incoming turbulence on the upward side of the obstacle, the quasi-stationary theory should be considered (Bearman & Fackrell 1975). However these theories are unable to predict correctly the high-frequency part of the pressure spectrum. It thus appears necessary to take into account the characteristics of the incoming stream in a more detailed manner. For this purpose Hunt (1973, 1975) and Durbin & Hunt (1980) have proposed an approach based on the hypothesis of rapid distortion of turbulence (Batchelor & Proudman 1954). They have applied it to the case of a bluff body (cross-stream characteristic dimension D) to calculate the high-frequency part of the pressure spectrum at the stagnation point. For any integral scale and in the high frequency range ($\tilde{f} \gg 1$) they obtained

$$S_{pp}(f) \propto \rho \overline{U}_\infty^2 u_\infty'^2 \exp(-\pi \tilde{f} q) \left(\frac{L_{11}}{D}\right)^{-\frac{2}{3}} D \tilde{f}^{-\frac{7}{3}}. \tag{1}$$

For large turbulent scales and low-frequency fluctuations $\tilde{f} \ll 1$ Hunt (1973) gives the following result for a circular cylinder of radius D:

$$S_{pp}(f) = \rho^2 \overline{U}_\infty^2 S_{uu}(f) [1 + \tfrac{1}{4} \tilde{f}^2 \log \tilde{f}^2]. \tag{2}$$

This formula is likely to be valid for any bluff body with modification of the constant $\frac{1}{4}$.

In the above expressions $S_{pp}(f)$ and $S_{uu}(f)$ represent the dimensional pressure and velocity spectra respectively, $\tilde{f}$ the non-dimensional frequency $\tilde{f} = 2\pi f D / \overline{U}_\infty$, L_{11} the integral scale of turbulence relative to the u-component of the velocity field and a longitudinal separation, and q is a constant that depends on the shape of the obstacle ($q = \frac{1}{2}$ for a circular cylinder). Thus, at low frequencies the pressure spectrum should be proportional to the velocity spectrum whereas at high frequencies Hunt's theory predicts an exponential decrease with frequency.

The purpose of the present study is to analyse in detail the mean and fluctuating pressure fields that exist at the surface of a cylinder of square cross-section placed in a turbulent stream with variable characteristics. Experimental results obtained previously (notably by Lee 1975) are extended by the use of a wide range of turbulent scales and intensities and numerous pressure transducers distributed over the surface of the prism. Special attention was paid in our experiment to discriminate between effects of turbulence intensity and scale. In particular all measurements were taken

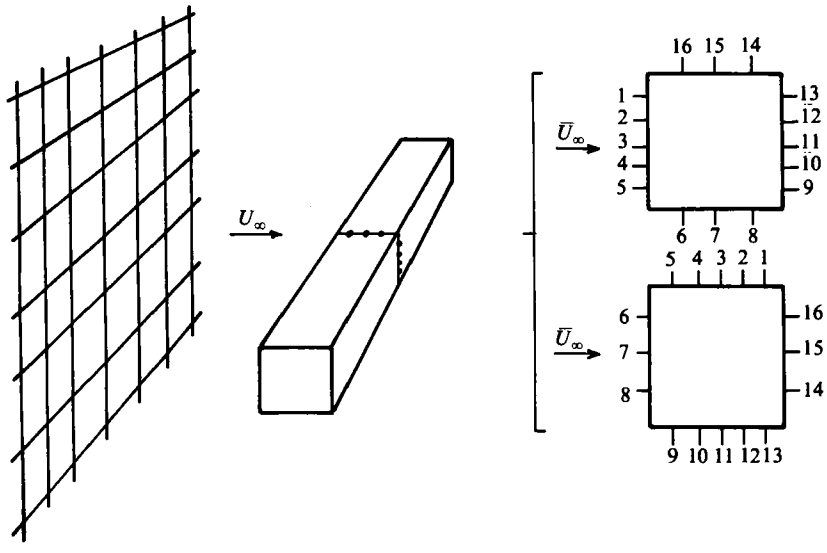

FIGURE 1. Pressure transducers' locations.

for constant blockage ratio (4.2%) and aspect ratio (20). Moreover the pressure measurements have tested Hunt's theory, and have improved understanding of the mechanism responsible to the fluctuating field.

2. Experimental conditions

The experiments were performed in a wind tunnel with a 1 m wide and 1.2 m high working section (Huot, Arbey & Rey 1983). The obstacle was a cylinder with square cross-section with sides of 5 cm (figure 1). This dimension was chosen to give the smallest blockage coefficient (4.2 %), and the longest aspect ratio (20), compatible with both the size of the working section and the need to install a sufficient number of transducers. Two 25 cm diameter disks, fitted to the extremities of the obstacle, were fitted to avoid any interaction with the boundary layers of the sidewalls. The mean velocity of the flow was $\bar{U}_\infty = 8.5$ m/s, which corresponds to a Reynolds number of $Re = 3 \times 10^4$. Due to the influence of the incoming turbulence, this Reynolds number was sufficient to obtain the transition in the boundary layer on the facing side (Sadeh & Brauer 1978).

Different square-mesh grids with a solidity of 0.3 and mesh sizes $M = 5$, 10 and 20 cm, were placed upstream of the cylinder. They were used to produce an homogeneous and quasi-isotropic turbulent flow, the scale and intensity of which could be adjusted by the choice of mesh size and distance from the grid. The characteristic components of the incoming turbulence were measured with a DISA cross-wire probe. The evolution of turbulence intensity $u'/\bar{U}_\infty$ and scale L_{11}/M with distance x/M from the grid are given by

$$\frac{u'}{\bar{U}_\infty} = 0.24\left(\frac{x}{M} - 3.5\right)^{-0.625}, \tag{3}$$

$$\frac{L_{11}}{M} = 0.14\left(\frac{x}{M} - \frac{x_0}{M}\right)^{0.4} \tag{4}$$

(in the above expressions x_0/M is a fictitious origin with value 2; 4; 3.5 for 5 cm, 10 cm, 20 cm mesh sizes respectively). Formula (3) is very close to the one obtained by Comte-Bellot & Corrsin (1971). The above results prove that it is possible to obtain, for the same turbulent intensity, three different integral scales, and to study their respective influences separately. For example, for $x/M = 20$, $u'/\bar{U}_\infty = 4.2\,\%$ and the corresponding ratio L_{11}/D varies from 0.4 to 1.7 with the 5 cm and 20 cm mesh size respectively. This set-up enables us to obtain a wide range of turbulent intensities and scales: $u'/\bar{U}_\infty$ varies from 3 to 17.5 % and L_{11}/D from 0.1 to 2. Note, however, that there was probably a non-uniformity of the turbulence near the mesh for $x/M \lesssim 10$.

To explore the mean pressure field on the obstacle, 0.6 mm pressure holes were distributed over its surface: 15 along the span, and 28 in a cross-section, 7 on each side. Mean pressures were measured with reference to the static pressure taken inside the working section. In addition, in order to measure the fluctuating pressure field, 16 miniature electret microphones WM 064, were incorporated in the sides of the prism, in the same cross-section. Their distribution is indicated on figure 1. For most of the experiments, the upstream face is the one where pressure transducers 1–5 are located. However, in some cases, in order to obtain a better description of the pressure field on the lateral sides, the obstacle was rotated by 90°, with the side bearing microphones 6, 7, 8 then facing upstream. To avoid confusion when interpreting the results, the location of the concerned transducers is indicated on each figure. The sensitivity of these transducers is of the order of 10 mV/Pa and their frequency response is linear between 3 Hz and 5 kHz (Huot 1980).

The fluctuating forces exerted on a section were measured in the following manner. For the drag, the transducers on the facing and lee sides were used. The pressure signals were then added together to give the force on the facing side: u_{s1} and on the lee side u_{s2}. The fluctuating drag was calculated by taking the difference between u_{s1} and u_{s2}. The fluctuating lift was obtained by the same procedure, with the prism rotated by 90°.

The spectra, cross-spectra and coherence functions were obtained with a two-channel spectrum analyser Nicolet 660 A.

3. Experimental results

3.1. *Mean pressure field on the obstacle*

Figure 2 presents, for different mesh sizes, the evolution with distance x/M from the grid, of the turbulence intensity $u'/\bar{U}_\infty$, the turbulence scale L_{11} and the mean pressure coefficient $C_{\bar{p}_b}$ measured in the middle of the lee side. For each value of x/M, that is for the same turbulence intensity, one can compare the values for $C_{\bar{p}_b}$ obtained for different mesh sizes, that is for different turbulence scales. This type of representation emphasizes the large influence of turbulence intensity on $C_{\bar{p}_b}$, and the lack of influence of turbulence scales. These results are analogous to those obtained by Petty (1979), with blocking conditions comparable to ours, but with larger turbulent scales.

Following Laneville, Gartshore & Parkinson, the evolution of the mean pressure coefficient on the rear side of the prism can be explained in the following way: the value of $C_{\bar{p}}$b depends on the curvature of the free shear layers, the stronger the curvature, the larger the depression on the lee side. External turbulence increases the entrainment of fluid from the recirculation zone into the free shear layers and hence

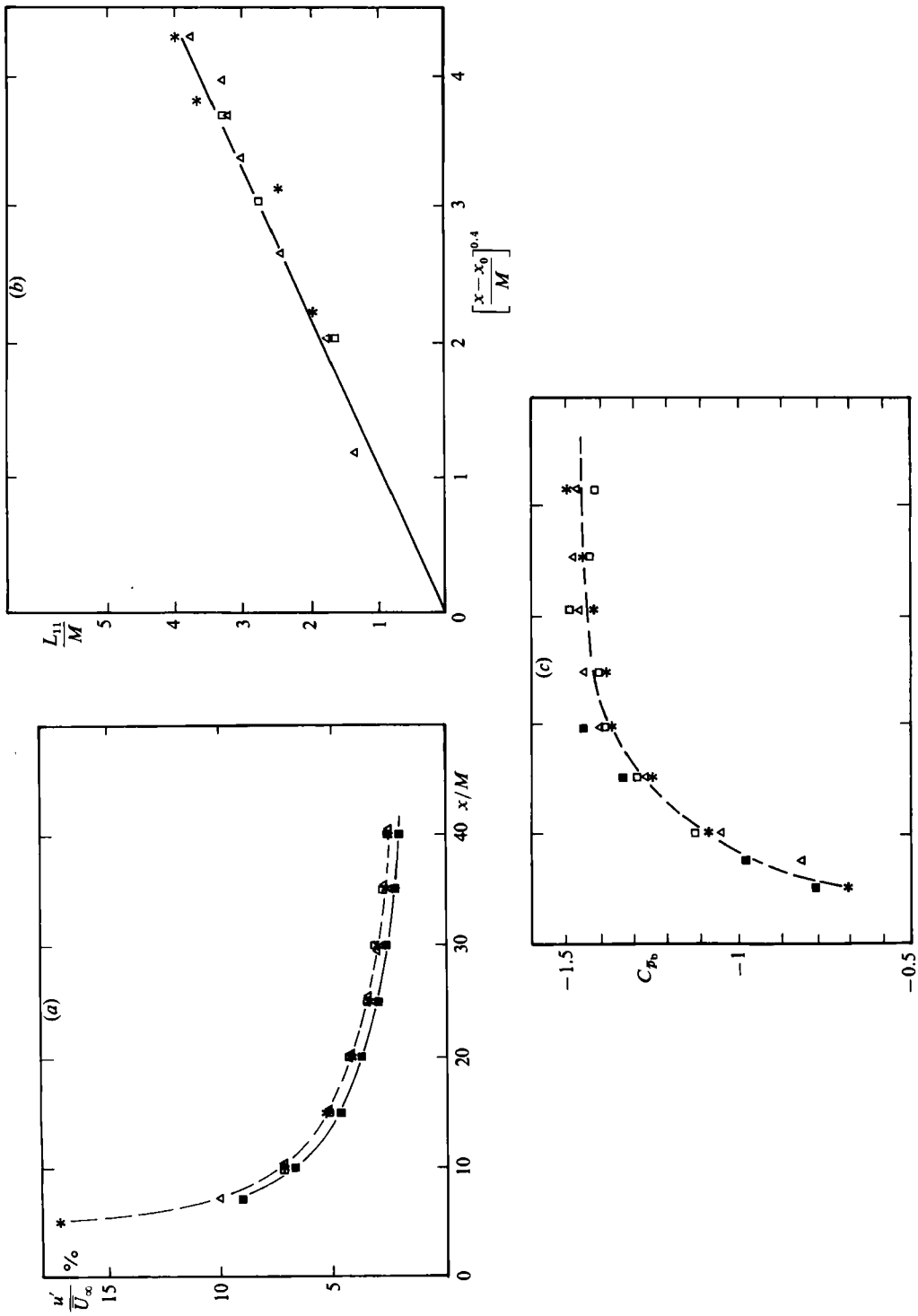

FIGURE 2. Evolution, with distance x/M from the grid, of: (*a*) the turbulence intensity u'/U_∞; *, $M = 5$ cm; □, 10 cm; △, 20 cm; ■, Comte-Bellot & Corrsin (1971). (*b*) the turbulence scale L_{11}; *, $M = 5$ cm, $x_0/M = 2$; □, 10, 4; △, 20, 3.5. (*c*) the mean pressure coefficient C_{p_b} measured in the middle of the lee side: *, $M = 5$ cm; □, 10 cm; △, 20 cm; ■, Petty (1979).

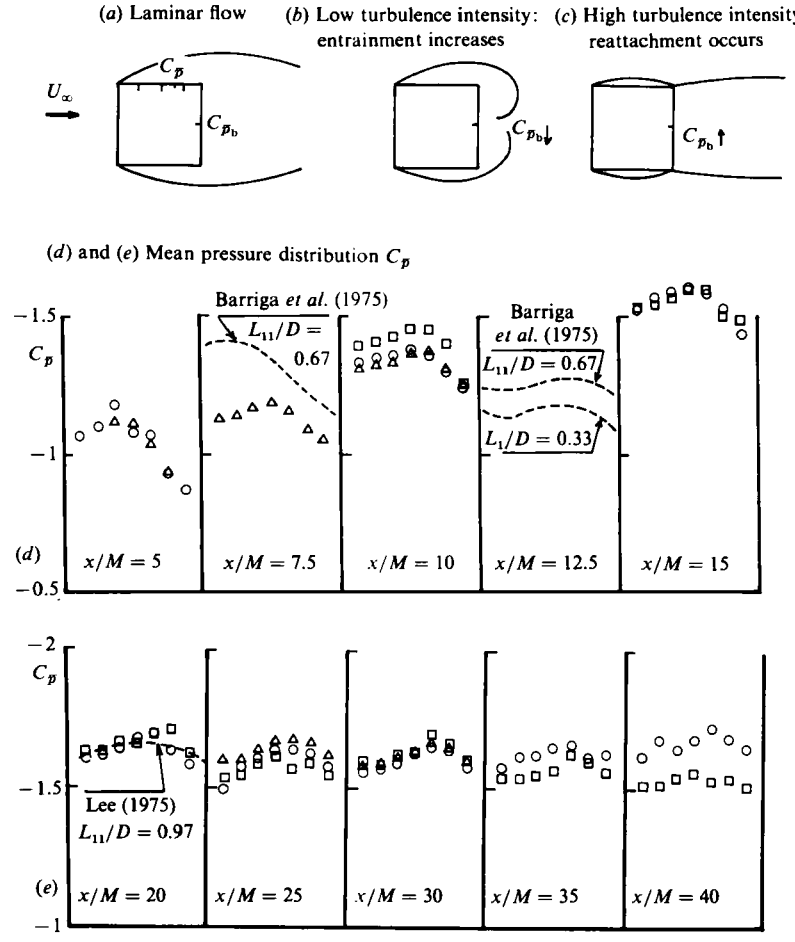

FIGURE 3. (*a*), (*b*), (*c*) Effect of the turbulence intensity on the curvature of the separated shear layer. (*d*), (*e*) Evolution, with distance x/M, of the mean pressure distribution C_p measured on the lateral side of the prism. ○, $M = 5$ cm; □, 10 cm; △, 20 cm.

increases their curvature and the depression on the lee side (figures 3*a* and *b*). When the entrainment becomes very large, the free shear layers eventually reattach to the side of the obstacle (figure 3*c*). Two new shear layers then separate at the rear edges, with weaker curvature as the reattachment point moves upstream, and the depression decreases. In practice, however, the increase in the depression on the lee side of the prism that should occur prior to reattachment (as suggested by figure 3*b*), is not observed.

The study of the mean pressure distribution along the lateral sides of the prism confirms these predictions (figures 3*d* and *e*). In fact, the experiments of Robertson *et al.* indicate that reattachment occurs a little upstream of the maximum of the mean pressure field. However, the uncertainty in the measurements does not permit us to draw definite conclusions regarding the respective influences of scale and turbulence intensity on the mean pressure repartition. Nonetheless the fact that only turbulence intensity increases entrainment is similar to the conclusions of Charnay, Mathieu & Comte-Bellot (1976) and Hillier & Cherry (1981).

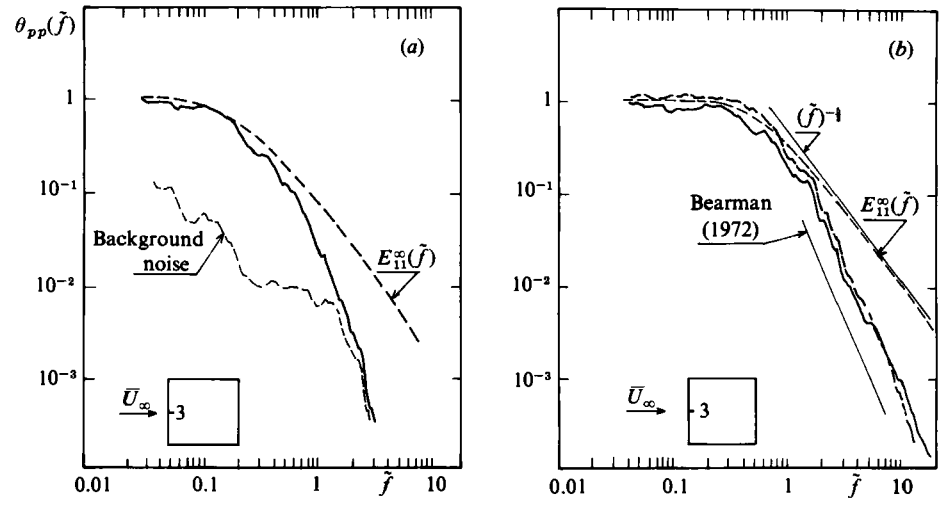

FIGURE 4. Comparison between the stagnation-point pressure spectrum, and the velocity spectrum measured upstream for different turbulence intensities. (*a*): $u'/\bar{U}_{\infty} = 3.1\,\%$, $L_{11}/D = 2$; (*b*) ——, $u'/\bar{U}_{\infty} = 17.5\,\%$, $L_{11}/D = 0.54$; – – – –, $u'/\bar{U}_{\infty} = 4.3\,\%$, $L_{11}/D = 0.44$.

The minor influence of turbulence scales on the mean depression on the lee side of the prism seems to indicate that it is not necessary to take into account the condition of geometric similarity of turbulent scales in a wind-tunnel experiment designed to measure the mean pressure field on a model. We shall see in the next paragraph that this is not the case for the fluctuating pressure field.

3.2. *Fluctuating pressure field on the obstacle*

3.2.1. *Pressure spectra measured at the stagnation point*

In order to test the validity of rapid distortion theory the pressure spectra were measured at the stagnation point of the flow for different values of intensity and scale of the incoming turbulence ($u'/\bar{U}_{\infty}$ varies from 3 to 17.5%, L_{11}/D from 0.1 to 2). A detailed study of the effect of intensity and scale was reported in another paper to which the reader is referred for additional information (Huot, Rey & Arbey 1984). We summarize here the main results of that study. Pressure spectra are drawn in the non-dimensional form used by Bearman (1972):

$$\theta_{pp}(\tilde{f}) = \frac{S_{pp}(f)}{4L_{11}\bar{U}_{\infty}u_{\infty}'^{2}\rho^{2}}; \quad \tilde{f} = \frac{2\pi f D}{\bar{U}_{\infty}}, \tag{5}$$

where $S_{pp}(f)$ is the measured spectrum and u'_{∞} the turbulence intensity existing far upstream of the obstacle (or in practice at the location of the obstacle, in its absence). This non-dimensional formulation allows a direct comparison between the pressure $\theta_{pp}(\tilde{f})$ and velocity spectra $E_{11}^{\infty}(\tilde{f})$ measured far upstream. In fact, at low frequencies the pressure spectrum is proportional to the velocity spectrum, which implies the superposition of the spectra $\theta_{pp}(\tilde{f})$ and $E_{11}^{\infty}(\tilde{f})$. This may be observed in figure 4 for the low-frequency range ($\tilde{f} < 0.25$), and various flow conditions. By contrast, at high frequencies, the pressure spectrum decreases more rapidly than the velocity spectrum (Huot *et al.* 1983, 1984). The observed rate of decrease ($\tilde{f}^{-2.95}$) is comparable to that obtained by Bearman (1972), for a stream with large-scale turbulence ($\tilde{f}^{-2.92}$), and to

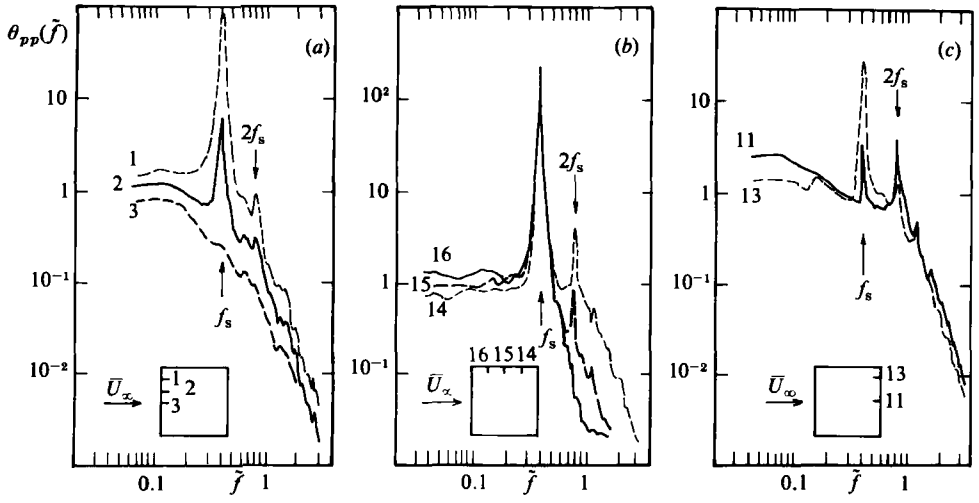

FIGURE 5. Comparison between the pressure spectrum measured at various locations on the prism: (*a*) facing side, (*b*) lateral side, (*c*) lee side ($u'/\bar{U}_\infty = 4.2\%$; $L_{11}/D = 1.7$).

that observed by Kawaī ($\tilde{f}^{-3}$). However this rate is smaller than that predicted by Hunt (see (2)). Note, on figure 4*a*, that for turbulence intensities lower than 3%, the background noise of the working section renders measurements of the high-frequency components of $\theta_{pp}(\tilde{f})$ inaccurate.

3.2.2. *Pressure spectra measured on the facing side*

An example of the pressure spectra $\theta_{pp}(\tilde{f})$ measured at different locations on the facing side is given in figure 5*a*. These spectra have been non-dimensionalized using the low-frequency value of the pressure spectrum obtained at the stagnation point. They show that $\theta_{pp}(\tilde{f})$ measured at the stagnation point (transducer 3) does not include any significant component at the Strouhal frequency f_S. But the influence of vortex shedding is felt more strongly as the distance from the edge of the obstacle decreases (transducer 1), when the existence of a very high peak at f_S and its harmonic $2f_S$ become apparent. However these peaks are sufficiently narrow to substantiate Hunt's assumption that the pressure fluctuations associated with vortex shedding can be decoupled from the broadband component.

3.2.3. *Pressure spectra measured on the lateral sides*

For points located on the lateral side (figure 5*b*), the Strouhal peak dominates the broadband component of the pressure spectrum. The amplitude of this peak decreases when the turbulence intensity is greater than 7%, but it is never observed to disappear completely, even for intensities as high as 17.5%.

The evolution, with the distance from the separation edge, of the broadband component of $\theta_{pp}(\tilde{f})$, is characterized by a decrease at low frequencies and an increase in the high-frequency range (as shown on figure 5*b* for a small turbulence intensity). When the turbulence intensity increases, a greater decrease is observed at low frequencies. As will be explained later (see also Cherry, Hillier & Latour 1984) the low-frequency level of θ_{pp} is induced by velocity fluctuations in the recirculation zone. For relatively small turbulence intensities (figure 5*b*) reattachment does not occur and the recirculation region extends over the whole length of the lateral side. The

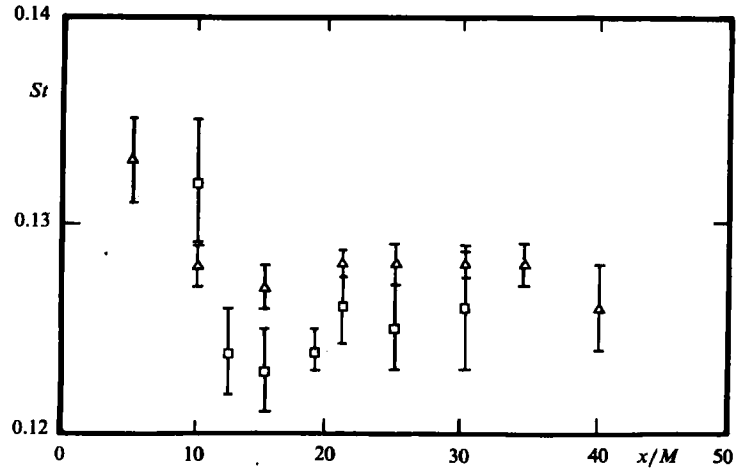

FIGURE 6. Variation of the Strouhal number with the distance x/M. Vertical bars indicate the uncertainty associated with the measurements: △, $M = 5$ cm; □, 20 cm.

pressure transducers located on this side are all affected in an identical manner, and mainly record the low-frequency fluctuations associated with the recirculation.

When the turbulent intensity grows, a reattachment of the shear layers occurs on the lateral side of the prism. The transducers upstream of the reattachment point, near the separation edge, are in the recirculation zone and so their spectra are dominated by low-frequency fluctuations. On the other hand pressure transducers further downstream are in the reattached zone, and so their spectra contain fewer low-frequency fluctuations. If one assumes (as indicated by the results of Robertson *et al.* 1979) that reattachment occurs slightly upstream of the static-pressure maximum, the results plotted on figure 3 indicate that only microphone 1 is in the recirculating zone, which is consistent with the high level of low-frequency fluctuations observed for that transducer.

The increase of the high-frequency level, with increasing distance from the edge, is easily explained by the gradual thickening of the free shear layer, which influences the pressure field on the lateral side.

3.2.4. *Pressure spectra measured on the lee side of the prism*

Pressure spectra measured on the lee side of the prism essentially show the existence of a second peak at twice the Strouhal frequency $2f_S$ whenever the turbulence intensity is less than 8% (figure 5*c*). For a microphone in the middle of the lee side, the level of this second peak is higher than that of the peak associated with f_S. This result can be explained by the antisymmetric nature of the fluctuating pressure field associated with vortex shedding.

3.3. *Evolution of Strouhal number with the turbulence characteristics of the incoming flow*

The evolution, with distance x/M from the grid and hence with turbulence intensity, of Strouhal number $St = f_S D/\overline{U}_\infty$ is shown on figure 6 for different values of the integral scale. The large uncertainty associated with the measurements does not allow any definite conclusion as to the respective influences of integral scale and turbulence intensity. However, the increase in the Strouhal number for high turbulence

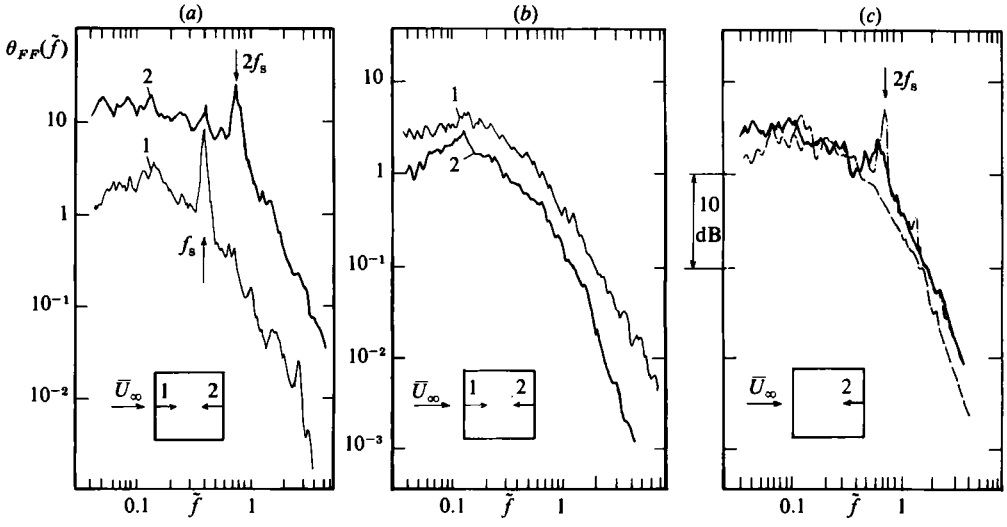

FIGURE 7. Spectra of the fluctuating pressure measured on the facing side (1) and on the lee side (2) for various turbulence intensities. (*a*) $u'/\bar{U}_\infty = 3.1\,\%$, $L_{11}/D = 2$; (*b*) $u'/\bar{U}_\infty = 17.5\,\%$, $L_{11}/D = 0.54$; (*c*) $M = 20$ cm; – – – –, $x/M = 5$; ——, 10; — · —, 15.

intensities corresponds to the increase of the pressure coefficient on the lee side of the prism and is due to the reattachment of the free shear layers on the sides of the prism.

3.4. *Measurement of the fluctuating forces on a section*

The study of the excitation of a structure by a turbulent stream makes it necessary to know the forces exerted on each section. The simple geometry of the square prism allows the direct integration of the pressure forces, to yield the fluctuating forces that act on a section. For this purpose, consider the following configuration:

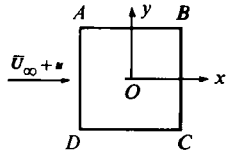

the Ox component of the force on the section $ABCD$ is given by

$$F_x = \int_D^A p(y, t)\,\mathrm{d}y - \int_C^B p(y, t)\,\mathrm{d}y, \tag{6}$$

where p is the local pressure. In the same way the component along Oy is given by

$$F_y = \int_D^C p(x, t)\,\mathrm{d}x - \int_A^B p(x, t)\,\mathrm{d}x. \tag{7}$$

To evaluate each of the integrals appearing in the expressions of these forces let us assume that

$$\int p(y, t)\,\mathrm{d}y = \sum_{i=1}^{n} p(y_i, t)\,\Delta y_i. \tag{8}$$

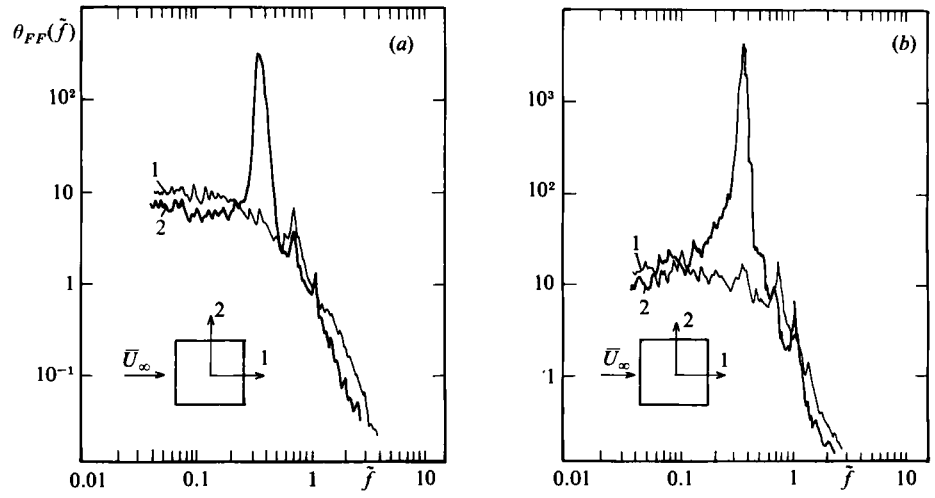

FIGURE 8. Spectra of the fluctuating drag (1) and lift (2) measured for different flow conditions. (*a*) $u'/\bar{U}_\infty = 5.3\,\%$, $L_{11}/D = 1.4$; (*b*) 3.1 %, 2.

If one takes equal Δy_i, the above expression becomes

$$\int p(y, t)\,\mathrm{d}y = \Delta y\Big(\sum_{i=1}^{n} p(y_i, t)\Big). \tag{9}$$

The calculation of the integral then reduces to the summation of n signals delivered by n transducers. This summation is performed with the experimental set-up described in §2. Such an integration yields the spectra for the fluctuating forces on the facing and lee sides, as well as the spectra for the fluctuating lift and drag.

Examination of figure 7 shows that, for turbulence intensities lower than 5 %, the main contribution to the fluctuating drag comes from pressure fluctuations on the lee side of the obstacle, whereas for turbulence intensities greater than 15 % the contributions from the upstream and rear side are comparable. Moreover, the comparison between pressure spectra, measured on the facing side (figure 5*a*) and the spectrum of the fluctuating force exerted on the same side and for the same turbulence conditions, shows a strong attenuation of the Strouhal peak, as observed in figure 7 (*a*). This phenomenon is a consequence of the antisymmetric behaviour of the pressure field induced by vortex shedding. An analogous result is obtained for the pressure field that develops on the lee side, as shown in figure 5 (*c*) and 7 (*c*).

The spectrum of the fluctuating lift essentially contains one peak at Strouhal frequency f_S, the amplitude of which increases with decreasing turbulence intensity, as shown in figures 8 (*a*) and (*b*) for different flow conditions. This result confirms the previous analysis of the pressure field induced on the prism. Finally, the equality between the broadband levels of the lift and drag spectra should be noticed.

To explain these phenomena, and to achieve a better understanding of the mechanisms that produce them, the amplitude and the phase of the cross-spectral densities for the pressure fluctuations have been measured at various locations on the obstacle.

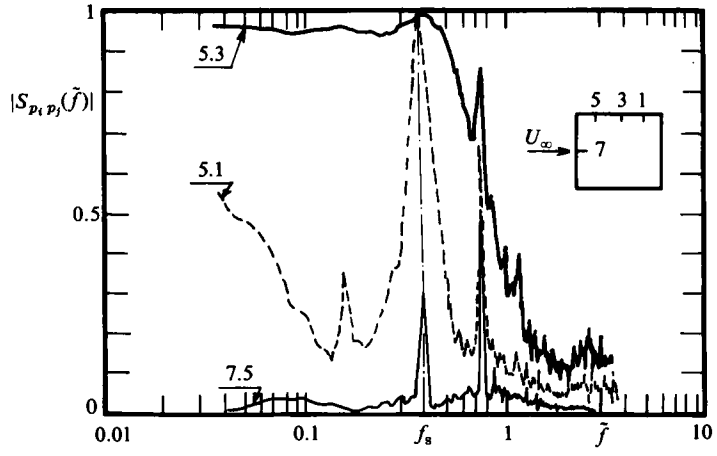

FIGURE 9. Coherence of the fluctuating pressure measured at various points of the same section ($u'/\overline{U}_\infty = 5.3\%$; $L_{11}/D = 1.4$).

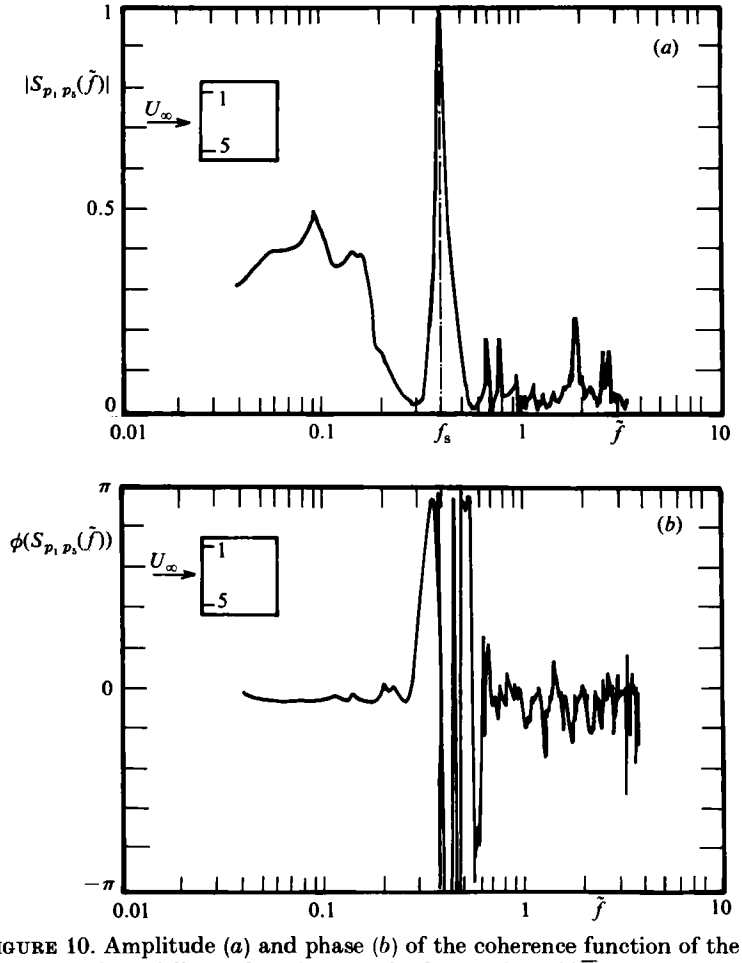

FIGURE 10. Amplitude (a) and phase (b) of the coherence function of the pressure field measured for different locations on the front side. ($u'/\overline{U}_\infty = 5.3\%$; $L_{11}/D = 1.4$).

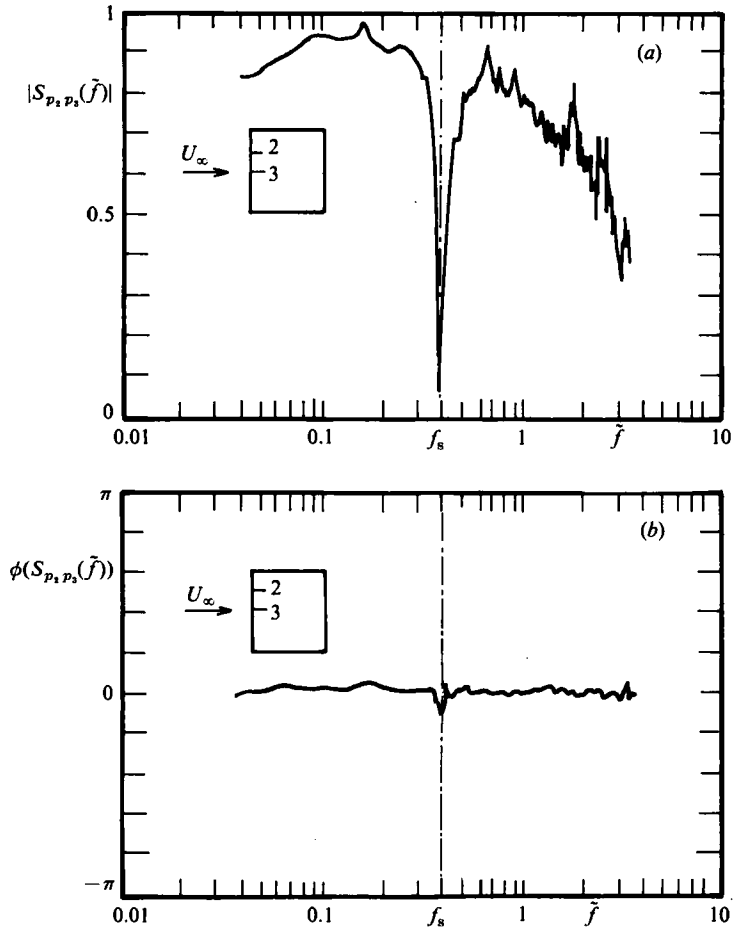

FIGURE 11. Amplitude (*a*) and phase (*b*) of the coherence function of the pressure field measured for different locations on the front side ($u'/\overline{U}_\infty = 5.3\%$; $L_{11}/D = 1.4$).

3.5. *Coherence and phase difference between transducers in the same cross-section*

Figure 9 shows that there is a low level of coherence between microphone 7 located at the stagnation point and microphone 5 located immediately after the separation edge on the lateral side, for a weak turbulence intensity. This result remains valid for higher turbulence intensities, and illustrates the small influence of the incoming turbulence on the pressure field at points in the recirculation zone. In addition, figure 9 also shows the strong coherence of the broadband component between transducer 5, near the separation edge, and 3, in the middle of the lateral side, for a weak turbulence intensity. However this coherence decreases when the turbulence intensity increases, which we interpret as being the result of the reattachment of the free shear layer that excludes transducer 3 from the recirculation zone. Finally, note that the weak coherence observed between transducers 5 and 1 is consistent with the increased influence of a thickened shear layer.

Figures 10 and 11 show the amplitude and phase of the coherence function measured for transducers on the front side. We note essentially the presence of a 180° phase shift at the Strouhal frequency f_S between the signals delivered by transducers

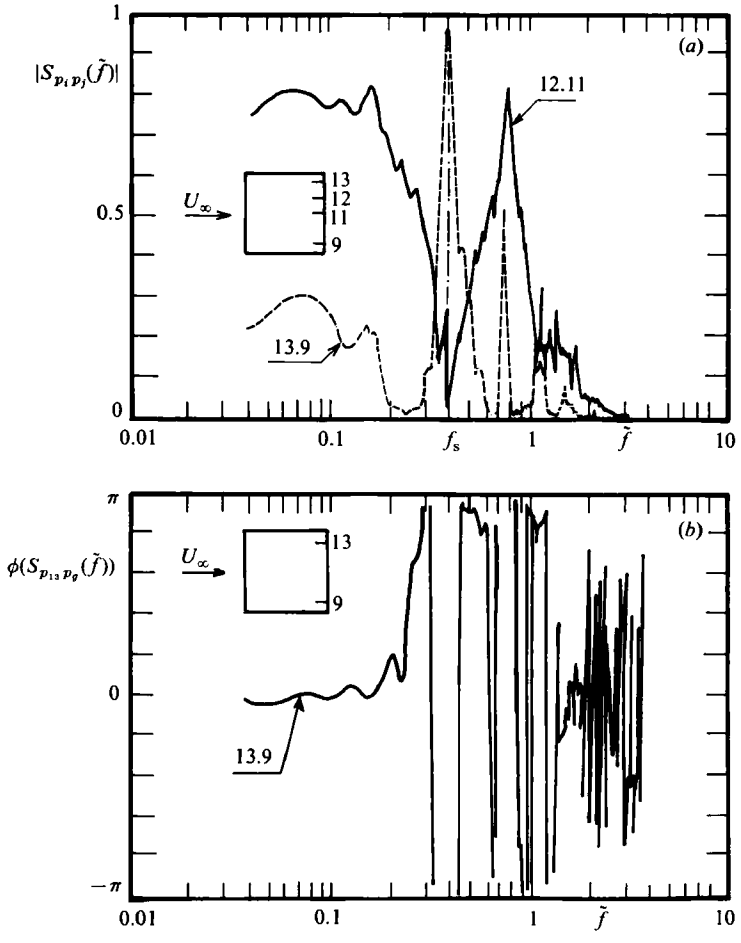

FIGURE 12. Amplitude (*a*) and phase (*b*) of the coherence function of the pressure field measured for different locations on the lee side ($u'/\overline{U}_\infty = 5.3\,\%$; $L_{11}/D = 1.4$).

1 and 5. This phase-shift demonstrates the antisymmetric nature of the pressure fluctuation induced by vortex shedding on the front side. This antisymmetry is also revealed by the lack of coherence measured between the central transducer 3 and the other transducers on the front side.

Similar behaviour is found on the rear side of the obstacle: figure 12 shows clearly the drop in the amplitude on the coherence function at Strouhal frequency f_S when one of the transducers is in the middle of the side. For the same frequency, a 180° phase shift may be noted between signals delivered by the transducers at the extreme edges of the rear side.

3.6. *Correlations measured along the span*

On figure 13 we compare the evolution, with distance x/M from the grid, of the non-dimensional correlation length R/D for the pressure field measured along the span on the lateral side. The essential feature is the strong decrease in the correlation length when the turbulence intensity increases, which confirms the results of Vickery and Lee.

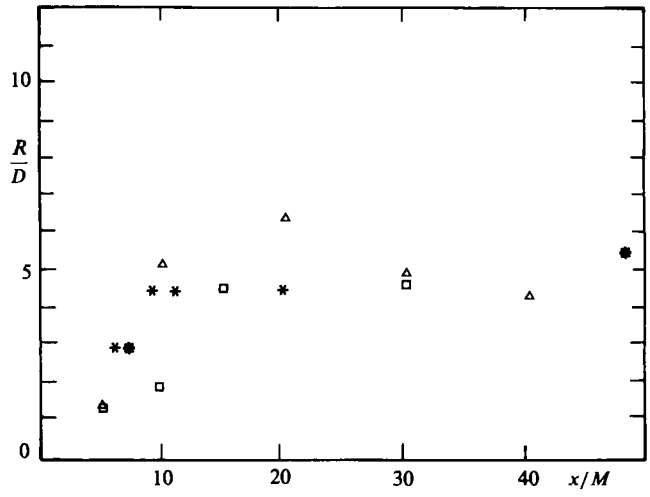

FIGURE 13. Variation of the correlation length of the pressure field with the distance from the grid x/M: △, $M = 5$ cm; □, 20 cm; ●, Vickery (1966) uniform flow; ∗, Lee (1975).

4. Conclusions

This study of the pressure field on a large-aspect-ratio prism placed in a turbulent flow has been conducted to allow the identification of the controlling mechanisms. First, a wide range of turbulence intensities and scales has been used to clarify their respective influence on the mean pressure field existing downstream of the separation point. The strong effect of the intensity, which leads to the decrease of the depression on the lee side of the obstacle, is interpreted as a consequence of the progressive reattachment of the free shear layers. However, the influence of the scale seems to be weaker. Secondly, the validity of Hunt's theory for the prediction of the pressure spectrum at the stagnation point is tested. At low frequencies the agreement between theory and measurement is excellent; but at high frequencies there is qualitative agreement in that the pressure spectrum rolls-off faster than the velocity spectrum and this divergence occurs for $\hat{f} > 1$. But quantitatively the predicted pressure is too low. Finally cross-spectra measurements of the pressure field, made at various locations on the prism, show that the pressure field developing downstream of the separation point is the result of two contributions: a quasi-sinusoidal component at the Strouhal frequency and a broadband component. The first contributions, induced by vortex shedding, has an antisymmetric behaviour pattern with respect to the symmetry plane of the flow. The second contribution, due to velocity fluctuations in the recirculation zone, is not directly influenced by the incoming turbulence.

One of the authors (H. Arbey) would like to thank Dr R. E. Britter for extensive discussions. This work has been supported by the C.N.R.S. under research contract: A.T.P. comportements mécaniques et thermiques dans les structures des bâtiments, no. 3697.

REFERENCES

BARRIGA, A. R., CROWE, C. T. & ROBERTSON, J. A. 1975 In *Proc. 4th Intl Conf. on Wind Effects on Building and Structures* (ed. K. J. Eaton), p. 89. Cambridge University Press.

BATCHELOR, G. K. & PROUDMAN, I. 1954 *Q. J. Mech. Appl. Maths* **2**, 83.

BEARMAN, P. W. 1972 *J. Fluid Mech.* **53**, 451.

BEARMAN, P. W. & FACKRELL, J. E. 1975 *J. Fluid Mech.* **72**, 229.

CHARNAY, G., MATHIEU, J. & COMTE-BELLOT, G. 1976 *Phys. Fluids* **19**, 1261.

CHERRY, N. J., HILLIER, R. & LATOUR, M. E. 1984 *J. Fluid Mech.* **114**, 13–46.

COMTE-BELLOT, G., CORRSIN, S. 1971 *J. Fluid Mech.* **48**, 273.

COURCHESNE, J. & LANEVILLE, A. 1982 *Trans. ASME* I: *J. Fluids Engng* **104**, 523–528.

DURBIN, P. A. & HUNT, J. C. R. 1980 *J. Fluid Mech.* **100**, 161.

HILLIER, R. & CHERRY, N. J. 1981 *J. Wind Engng and Ind. Aero.* **8**, 49.

HUNT, J. C. R. 1973 *J. Fluid Mech.* **61**, 627.

HUNT, J. C. R. 1975 *Proc. 4th Intl Conf. on Wind Effects on Building and Structures* (ed. K. J. Eaton), p. 309. Cambridge University Press.

HUOT, J. P. 1980 Thèse de Docteur-Ingénieur, Lyon.

HUOT, J. P., ARBEY, H. & REY, C. 1983 *C. R. Acad. Sci. Paris* **296**, 305.

HUOT, J. P., REY, C. & ARBEY, H. 1984 *Phys. Fluids* **27**, 541.

KAO, T. W. 1970 Thesis, University of Western Ontario.

KAWAI, H., KATSURA, J. & ISHIZAKI, H. 1980 *Wind Engineering*. Pergamon.

KWOK, K. C. S. 1983 *Trans. ASME* I: *J. Fluids Engng* **105**, 140.

LANEVILLE, A., GARTSHORE, J. S. & PARKINSON, G. V. 1975 *Proc. 4th Intl Conf. on Wind Effects on Buildings and Structures* (ed. K. J. Eaton), p. 333. Cambridge University Press.

LEE, B. E. 1975 *J. Fluid Mech.* **69**, 263.

PETTY, D. G. 1979 *J. Ind. Aerodyn.* **4**, 247.

RANGA RAJU, K. G., VIJAYA SINGH 1975 *J. Ind. Aerodyn.* **1**, 301.

ROBERTSON, J. M., WEDDING, J. B., PETERKA, J. A. & CERMAK, J. E. 1978 *J. Ind. Aerodyn.* **2**, 345.

SADEH, W. & BRAUER, H. J. 1978 *NASA C.R.* 3019.

VICKERY, B. J. 1966 *J. Fluid Mech.* **25**, 481.

WEDDING, J. B., ROBERTSON, J. M., PETERKA, J. A. & AKINS, R. E. 1978 *Trans ASME* I: *J. Fluids Engng* **100**, 485.